Computers and Structures 249 (2021) 106502

Contents lists available at ScienceDirect

Computers and Structures

journal homepage: www.elsevier.com/locate/compstruc

Accurate solution of wave propagation problems in elasticity

Ki-Tae Kim [a], Klaus-Jürgen Bathe [b,*]

[a] Department of Applied Mathematics, University of California, Merced, CA, United States
[b] Department of Mechanical Engineering, Massachusetts Institute of Technology, Cambridge, MA, United States

ARTICLE INFO

Article history:
Received 21 December 2020
Accepted 28 January 2021

Keywords:
Wave propagations in solids
Multiple waves
Overlapping finite elements
Bathe implicit time integration
Dispersion errors
Monotonic convergence

ABSTRACT

The accurate solution of wave propagations in general two- and three-dimensional solids is still difficult and frequently impossible to achieve with the current computational schemes and computers available. We present in this paper a solution scheme that has much promise for the accurate solution of wave propagations in general solids. The procedure is based on the use of "overlapping finite elements" and direct time integration. The overlapping finite elements are effective because the spatial dispersion error is relatively small and can be monotonically reduced using a finer mesh. Similarly, the time integration dispersion errors can also be reduced monotonically as the time step becomes smaller. Hence the key property of the solution scheme is that the total dispersion error in the simulation of multiple waves traveling through solids is monotonically reduced as the spatial discretization and time stepping become finer. We summarize the ingredients of the solution scheme and illustrate the characteristics in the solution of some wave propagation problems that are difficult to solve accurately. These solutions may be benchmark solutions to use in the evaluations of other computational schemes.

1. Introduction

Although much research has been expended on the solution of wave propagations in solids, the accurate solution of *multiple* waves traveling through complex domains of solids is still very difficult and may be impossible. Nevertheless, such solutions are much needed in various important areas of engineering and scientific endeavors. In engineering, for example, the accurate prediction of seismic waves is important in damage predictions, and also, for non-destructive evaluation, the accurate solution of waves would strengthen the developments of techniques. Both fields of engineering are very large and have become increasingly important. In the sciences, for example, wave propagations in medical applications and research are ubiquitous.

For the solutions of wave propagations, finite difference, finite element, spectral techniques, meshless methods, and discontinuous Galerkin schemes have been much researched and are used, see for the methods and some applications for example [1–16], and recently "overlapping" finite element methods have been proposed [17–21]. Finite difference methods can be used for general analyses of solids but there are difficulties in the discretization of complex domains and the solution errors can be large. Finite element methods exhibit much better generality in representing complex domains but the solution errors can also be large. The use of spectral techniques results in better solution accuracy but the representation of complex domains is difficult and may not be possible. Meshless techniques have more recently been proposed and can yield accurate solutions but the solution cost can be very high. Discontinuous finite element or Galerkin methods can be used quite generally to represent complex domains but these entail the use of penalty factors that are undesirable in engineering practice. In all these solution schemes, direct time integration is used most generally [4].

A good overall solution scheme for the numerical solution of wave propagations would be one, for which the following property holds: as the spatial discretization is increasingly refined and the time discretization is also refined, the solution should become increasingly more accurate. This requirement should hold for problems with multiple waves, irregular spatial meshes, and with no specific relationship to hold between the "size" of the spatial discretization and the "time step" of the time integration. Such a scheme would be attractive for use in practice because it would exhibit the same convergence property as effective spatial discretizations for static analyses [4]. However, the scheme would have to be also computationally efficient.

We recently proposed the use of "overlapping finite elements" [17–23] and the Bathe implicit direct time integration for the solution of wave propagations [20,21]. This solution approach provided accurate solutions to some illustrative problems and in particular

* Corresponding author.
E-mail address: kjb@mit.edu (K.J. Bathe).

https://doi.org/10.1016/j.compstruc.2021.106502
0045-7949/

exhibited in the solution of the problems the good property of convergence mentioned above.

We shall only consider the Bathe method of time integration in this paper, studies comparing the Bathe scheme with other methods have been amply published before [24–32].

Our objective in this paper is to summarize the complete solution scheme, give novel important insights with illustrations, and present the solutions of some difficult to solve wave propagations in elasticity. While we consider only the solution of two-dimensional problems, the solution scheme can in principle also be applied in three-dimensional analyses – however, for such applications a detailed assessment of the computational effort need still be conducted.

2. The problem considered

For a displacement field $\boldsymbol{u}(x,y,t)$ in a two-dimensional domain, the equations of motion for elastic wave propagations are, in linear analysis,

$$\rho\ddot{\boldsymbol{u}} = div\,\boldsymbol{\tau} + \boldsymbol{f}^B \tag{1}$$

in which ρ, $\boldsymbol{\tau}$ and $\boldsymbol{f}^B$ are the mass density, stress tensor and body force vector, respectively. The governing equation is subjected to two types of boundary conditions, the Dirichlet boundary condition on S_u

$$\boldsymbol{u} = \boldsymbol{u}^{S_u} \tag{2}$$

and the Neumann boundary condition on S_f

$$\boldsymbol{\tau}\cdot\boldsymbol{n} = \boldsymbol{f}^{S_f} \tag{3}$$

where **n** denotes the unit normal vector on the boundary S_f. Using the principle of virtual work, we obtain [4]

$$\int_V \bar{\boldsymbol{\varepsilon}}^T \boldsymbol{\tau}\,dV + \int_V \rho\bar{\boldsymbol{u}}^T\ddot{\boldsymbol{u}}\,dV = \int_V \bar{\boldsymbol{u}}^T\boldsymbol{f}^B\,dV + \int_{S_f}\bar{\boldsymbol{u}}^T\boldsymbol{f}^{S_f}\,dS_f \tag{4}$$

in which $\bar{\boldsymbol{u}}$ and $\bar{\boldsymbol{\varepsilon}}$ indicate the virtual displacement and the corresponding virtual strain, respectively, and V is the body volume considered.

Discretizing Eq. (4), we arrive at the following matrix form of the governing equations [4]

$$\boldsymbol{M}\ddot{\boldsymbol{U}} + \boldsymbol{C}\dot{\boldsymbol{U}} + \boldsymbol{K}\boldsymbol{U} = \boldsymbol{R} \tag{5}$$

where **M**, **C** and **K** are the mass, damping and stiffness matrices, **R** is the load vector, **U** is the nodal displacement vector, and an over-dot denotes a time derivative. In our wave propagation solutions we assume that no physical damping effects are present, hence **C = 0.**

3. The overlapping finite element scheme

We consider the 3-node triangular overlapping elements enriched for 2D wave propagation problems [20]. The same concepts described here can be directly extended for the formulation of 4-node quadrilateral overlapping elements and the corresponding 3D elements [22,23], and these elements can be used in conjunction with AMORE, the scheme of Automatic Meshing with Overlapping and Regular Elements [18].

In the overlapping finite element method, the displacement variable $\boldsymbol{u} = [u_1, u_2]^T$ is for element K with nodes I, L, M interpolated as

$$\boldsymbol{u}_h(\boldsymbol{x}) = h_I\boldsymbol{\psi}_I(\boldsymbol{x}) + h_L\boldsymbol{\psi}_L(\boldsymbol{x}) + h_M\boldsymbol{\psi}_M(\boldsymbol{x}) \tag{6}$$

where $\boldsymbol{x} = [x,y]^T$, and the h_I, h_L, h_M are the shape functions of the traditional 3-node element. The function $\boldsymbol{\psi}_I$ is defined as

$$\boldsymbol{\psi}_I(\boldsymbol{x}) = \sum_{J=I,\,L,\,M}\phi_J^I\boldsymbol{u}_J;\quad \boldsymbol{u}_J = p_n\,\boldsymbol{a}_{Jn} \tag{7}$$

where ϕ_J^I is a partition of unity function approximated by a quadratic polynomial (see Refs. [18,19] for details), p_n is a set of local basis functions and the $\boldsymbol{a}_{Jn}$ are the corresponding unknown coefficients.

For the solution of 2D wave propagation problems, the bi-linear polynomial functions and trigonometric functions are employed for the local basis, namely, we use, with a local Cartesian coordinate system (x,y),

$$[p_1,p_2,\cdots] = \begin{bmatrix} 1,x,y,xy, \\ \cos\left(\frac{2\pi x}{\lambda_x}\right),\sin\left(\frac{2\pi x}{\lambda_x}\right),\cos\left(\frac{2\pi y}{\lambda_y}\right),\sin\left(\frac{2\pi y}{\lambda_y}\right), \\ \cos\left(\frac{2\pi x}{\lambda_x}+\frac{2\pi y}{\lambda_y}\right),\sin\left(\frac{2\pi x}{\lambda_x}+\frac{2\pi y}{\lambda_y}\right),\cos\left(\frac{2\pi x}{\lambda_x}-\frac{2\pi y}{\lambda_y}\right),\sin\left(\frac{2\pi x}{\lambda_x}-\frac{2\pi y}{\lambda_y}\right), \\ \cos\left(2\cdot\frac{2\pi x}{\lambda_x}\right),\sin\left(2\cdot\frac{2\pi x}{\lambda_x}\right),\cos\left(2\cdot\frac{2\pi y}{\lambda_y}\right),\sin\left(2\cdot\frac{2\pi y}{\lambda_y}\right), \\ \cos\left(2\cdot\frac{2\pi x}{\lambda_x}+2\cdot\frac{2\pi y}{\lambda_y}\right),\sin\left(2\cdot\frac{2\pi x}{\lambda_x}+2\cdot\frac{2\pi y}{\lambda_y}\right),\cos\left(2\cdot\frac{2\pi x}{\lambda_x}-2\cdot\frac{2\pi y}{\lambda_y}\right),\sin\left(2\cdot\frac{2\pi x}{\lambda_x}-2\cdot\frac{2\pi y}{\lambda_y}\right), \\ \cdots \end{bmatrix} \tag{8}$$

where λ_x and λ_y are the fundamental wavelengths in the x- and y-directions, respectively, and, for example, the order of the trigonometric function used for the x-axis direction in the basis is the coefficient multiplying $\frac{2\pi x}{\lambda_x}$. The use of the bi-linear polynomial function ensures the linear consistency (reproducing the linear fields like rigid body modes and constant strain states), and the trigonometric polynomial basis enhances the solution accuracy for the Helmholtz equation (the time-independent form of the wave equation).

An important point for the overlapping finite elements with the bi-linear polynomial and the trigonometric functions up to order n (we shall refer to them as OFE-TRIn) is that the dispersion error caused by the OFE-TRIn discretization is negligible and almost independent of the propagation direction, for wave modes with $k_h h/\pi < n$ where k_h is the numerical wave number and h is the typical size of overlap region. This implies that when used with the implicit direct time integration methods, the OFE-TRIn exhibits the monotonic convergence of the solution with refining the spatial discretization and/or the time discretization.

4. The Bathe time integration scheme

The Bathe time integration scheme was originally published for nonlinear analyses [24,25] but then further researched and also proposed for linear structural and wave propagation solutions [26–31]; and it is now in essence a family of schemes. All techniques provide implicit time integrations and use two sub-steps for the integration over the time step Δt. We shall use in this paper the standard Bathe time integration scheme (also referred to as the γ-Bathe scheme, because γ can be a variable) [25,26] and the β_1/β_2-Bathe scheme in which γ, β_1 and β_2 are variables but β_2 is usually set by the choice of β_1 [28,31]. All these schemes can be derived from the ρ_∞-Bathe method [29]. An explicit scheme using the same approach has been presented in Ref. [32].

4.1. The standard implicit γ-Bathe scheme

In the Bathe method, well-known integration schemes are used for each sub-step [4]. In the first sub-step, we utilize the trapezoidal rule, or more generally, the Newmark method

$${}^{t+\gamma\Delta t}\dot{\boldsymbol{U}} = {}^t\dot{\boldsymbol{U}} + \left[(1-\delta)\;{}^t\ddot{\boldsymbol{U}} + \delta\;{}^{t+\gamma\Delta t}\ddot{\boldsymbol{U}}\right]\gamma\Delta t \tag{9}$$

$${}^{t+\gamma\Delta t}\boldsymbol{U} = {}^t\boldsymbol{U} + {}^t\dot{\boldsymbol{U}}\gamma\Delta t + \left[\left(\frac{1}{2}-\alpha\right){}^t\ddot{\boldsymbol{U}} + \alpha\,{}^{t+\gamma\Delta t}\ddot{\boldsymbol{U}}\right]\gamma^2\Delta t^2 \tag{10}$$

and in the second sub-step, we utilize the Euler 3-point backward rule

$$ {}^{t+\Delta t}\dot{\boldsymbol{U}} = c_1\,{}^{t}\boldsymbol{U} + c_2\,{}^{t+\gamma\Delta t}\boldsymbol{U} + c_3\,{}^{t+\Delta t}\boldsymbol{U} \tag{11}$$

$$ {}^{t+\Delta t}\ddot{\boldsymbol{U}} = c_1\,{}^{t}\dot{\boldsymbol{U}} + c_2\,{}^{t+\gamma\Delta t}\dot{\boldsymbol{U}} + c_3\,{}^{t+\Delta t}\dot{\boldsymbol{U}} \tag{12}$$

where

$$ c_1 = \frac{1-\gamma}{\gamma\Delta t},\quad c_2 = \frac{-1}{(1-\gamma)\gamma\Delta t},\quad c_3 = \frac{2-\gamma}{(1-\gamma)\Delta t} \tag{13}$$

Considering linear analysis, the equilibrium equations applied at time $t+\gamma\Delta t$ and time $t+\Delta t$ are

$$ \boldsymbol{M}\,{}^{t+\gamma\Delta t}\ddot{\boldsymbol{U}} + \boldsymbol{C}\,{}^{t+\gamma\Delta t}\dot{\boldsymbol{U}} + \boldsymbol{K}\,{}^{t+\gamma\Delta t}\boldsymbol{U} = {}^{t+\gamma\Delta t}\boldsymbol{R} \tag{14}$$

$$ \boldsymbol{M}\,{}^{t+\Delta t}\ddot{\boldsymbol{U}} + \boldsymbol{C}\,{}^{t+\Delta t}\dot{\boldsymbol{U}} + \boldsymbol{K}\,{}^{t+\Delta t}\boldsymbol{U} = {}^{t+\Delta t}\boldsymbol{R} \tag{15}$$

Using the relations in Eqs. (9)–(13) with the equilibrium equations at the two time points, Eqs. (14) and (15), we construct the time-stepping equations as

$$ \widehat{\boldsymbol{K}}_1\,{}^{t+\gamma\Delta t}\boldsymbol{U} = \widehat{\boldsymbol{R}}_1 \tag{16}$$

$$ \widehat{\boldsymbol{K}}_2\,{}^{t+\Delta t}\boldsymbol{U} = \widehat{\boldsymbol{R}}_2 \tag{17}$$

where

$$ \widehat{\boldsymbol{K}}_1 = \frac{1}{\alpha\gamma^2\Delta t^2}\boldsymbol{M} + \frac{\delta}{\alpha\gamma\Delta t}\boldsymbol{C} + \boldsymbol{K} \tag{18}$$

$$ \widehat{\boldsymbol{K}}_2 = c_3^2\boldsymbol{M} + c_3\boldsymbol{C} + \boldsymbol{K} \tag{19}$$

$$ \begin{aligned} \widehat{\boldsymbol{R}}_1 = {}&{}^{t+\gamma\Delta t}\boldsymbol{R} + \boldsymbol{M}\left(\left(\frac{1}{2\alpha}-1\right){}^{t}\ddot{\boldsymbol{U}} + \frac{1}{\alpha\gamma\Delta t}\,{}^{t}\dot{\boldsymbol{U}} + \frac{1}{\alpha\gamma^2\Delta t^2}\,{}^{t}\boldsymbol{U}\right) \\ &+ \boldsymbol{C}\left(\frac{(\delta-2\alpha)\gamma\Delta t}{2\alpha}\,{}^{t}\ddot{\boldsymbol{U}} + \left(\frac{\delta}{\alpha}-1\right){}^{t}\dot{\boldsymbol{U}} + \frac{\delta}{\alpha\gamma\Delta t}\,{}^{t}\boldsymbol{U}\right) \end{aligned} \tag{20}$$

$$ \begin{aligned} \widehat{\boldsymbol{R}}_2 = {}&{}^{t+\Delta t}\boldsymbol{R} - \boldsymbol{M}\left(c_1c_3\,{}^{t}\boldsymbol{U} + c_2c_3\,{}^{t+\gamma\Delta t}\boldsymbol{U} + c_1\,{}^{t}\dot{\boldsymbol{U}} + c_2\,{}^{t+\gamma\Delta t}\dot{\boldsymbol{U}}\right) \\ &- \boldsymbol{C}\left(c_1\,{}^{t}\boldsymbol{U} + c_2\,{}^{t+\gamma\Delta t}\boldsymbol{U}\right) \end{aligned} \tag{21}$$

In general, the trapezoidal rule ($\alpha = 1/4$, $\delta = 1/2$) is used in the first sub-step and we shall always do so in this paper. For the time step subdivision, mostly $\gamma = 1/2$ or $\gamma = 2-\sqrt{2}$ (because then in linear analysis $\widehat{\boldsymbol{K}}_1 = \widehat{\boldsymbol{K}}_2$), have been used but γ can vary and then different accuracy properties are reached [26,32].

4.2. The β_1/β_2-Bathe implicit time integration method

We now use for the first sub-step

$$ {}^{t+\gamma\Delta t}\dot{\mathbf{U}} = -\frac{2}{(\gamma\Delta t)}\,{}^{t}\mathbf{U} - {}^{t}\dot{\mathbf{U}} + \frac{2}{(\gamma\Delta t)}\,{}^{t+\gamma\Delta t}\mathbf{U} \tag{22}$$

$$ {}^{t+\gamma\Delta t}\ddot{\mathbf{U}} = -\frac{4}{(\gamma\Delta t)^2}\,{}^{t}\mathbf{U} - \frac{4}{(\gamma\Delta t)}\,{}^{t}\dot{\mathbf{U}} - {}^{t}\ddot{\mathbf{U}} + \frac{4}{(\gamma\Delta t)^2}\,{}^{t+\gamma\Delta t}\mathbf{U} \tag{23}$$

Substituting from Eqs. (22) and (23) into Eq. (14), we obtain

$$ \widehat{\mathbf{K}}_1\,{}^{t+\gamma\Delta t}\mathbf{U} = {}^{t+\gamma\Delta t}\widehat{\mathbf{R}}_1 \tag{24}$$

where

$$ \widehat{\mathbf{K}}_1 = \frac{4}{(\gamma\Delta t)^2}\mathbf{M} + \frac{2}{(\gamma\Delta t)}\mathbf{C} + \mathbf{K} \tag{25}$$

$$ \begin{aligned} {}^{t+\gamma\Delta t}\widehat{\mathbf{R}}_1 = {}&{}^{t+\gamma\Delta t}\mathbf{R} + \mathbf{M}\left[\frac{4}{(\gamma\Delta t)^2}\,{}^{t}\mathbf{U} + \frac{4}{\gamma\Delta t}\,{}^{t}\dot{\mathbf{U}} + {}^{t}\ddot{\mathbf{U}}\right] \\ &+ \mathbf{C}\left[\frac{2}{\gamma\Delta t}\,{}^{t}\mathbf{U} + {}^{t}\dot{\mathbf{U}}\right] \end{aligned} \tag{26}$$

For the second sub-step, the governing equations are

$$ \begin{aligned} {}^{t+\Delta t}\dot{\mathbf{U}} = {}&-\frac{1}{\beta_2(1-\gamma)\Delta t}\,{}^{t}\mathbf{U} - \frac{\gamma(1-\beta_1)}{\beta_2(1-\gamma)}\,{}^{t}\dot{\mathbf{U}} \\ &- \frac{\gamma\beta_1 + (1-\beta_2)(1-\gamma)}{\beta_2(1-\gamma)}\,{}^{t+\gamma\Delta t}\dot{\mathbf{U}} + \frac{1}{\beta_2(1-\gamma)\Delta t}\,{}^{t+\Delta t}\mathbf{U} \end{aligned} \tag{27}$$

$$ \begin{aligned} {}^{t+\Delta t}\ddot{\mathbf{U}} = {}&-\frac{1}{(\beta_2(1-\gamma)\Delta t)^2}\,{}^{t}\mathbf{U} - \frac{\gamma(1-\beta_1)+\beta_2(1-\gamma)}{(\beta_2(1-\gamma))^2\Delta t}\,{}^{t}\dot{\mathbf{U}} \\ &- \frac{\gamma(1-\beta_1)}{\beta_2(1-\gamma)}\,{}^{t}\ddot{\mathbf{U}} - \frac{\gamma\beta_1+(1-\beta_2)(1-\gamma)}{(\beta_2(1-\gamma))^2\Delta t}\,{}^{t+\gamma\Delta t}\dot{\mathbf{U}} \\ &- \frac{\gamma\beta_1+(1-\beta_2)(1-\gamma)}{\beta_2(1-\gamma)}\,{}^{t+\gamma\Delta t}\ddot{\mathbf{U}} \\ &+ \frac{1}{(\beta_2(1-\gamma)\Delta t)^2}\,{}^{t+\Delta t}\mathbf{U} \end{aligned} \tag{28}$$

Substituting from Eqs. (27) and (28) into Eq. (15) we obtain

$$ \widehat{\mathbf{K}}_2\,{}^{t+\Delta t}\mathbf{U} = {}^{t+\Delta t}\widehat{\mathbf{R}}_2 \tag{29}$$

where

$$ \widehat{\mathbf{K}}_2 = \frac{1}{(\beta_2(1-\gamma)\Delta t)^2}\mathbf{M} + \frac{1}{\beta_2(1-\gamma)\Delta t}\mathbf{C} + \mathbf{K} \tag{30}$$

and

$$ \begin{aligned} {}^{t+\Delta t}\widehat{\mathbf{R}}_2 = {}&{}^{t+\Delta t}\mathbf{R} + \mathbf{M}\left[\frac{1}{(\beta_2(1-\gamma)\Delta t)^2}\,{}^{t}\mathbf{U} + \frac{\gamma(1-\beta_1)+\beta_2(1-\gamma)}{(\beta_2(1-\gamma))^2\Delta t}\,{}^{t}\dot{\mathbf{U}}\right. \\ &+ \frac{\gamma\beta_1+(1-\beta_2)(1-\gamma)}{(\beta_2(1-\gamma))^2\Delta t}\,{}^{t+\gamma\Delta t}\dot{\mathbf{U}} + \frac{\gamma(1-\beta_1)}{\beta_2(1-\gamma)}\,{}^{t}\ddot{\mathbf{U}} \\ &\left.+ \frac{\gamma\beta_1+(1-\beta_2)(1-\gamma)}{\beta_2(1-\gamma)}\,{}^{t+\gamma\Delta t}\ddot{\mathbf{U}}\right] + \mathbf{C}\left[\frac{1}{\beta_2(1-\gamma)\Delta t}\,{}^{t}\mathbf{U}\right. \\ &\left.+ \frac{\gamma(1-\beta_1)}{\beta_2(1-\gamma)}\,{}^{t}\dot{\mathbf{U}} + \frac{\gamma\beta_1+(1-\beta_2)(1-\gamma)}{\beta_2(1-\gamma)}\,{}^{t+\gamma\Delta t}\dot{\mathbf{U}}\right] \end{aligned} \tag{31}$$

In this paper, we shall use $\gamma = 0.5$ and $\beta_1 = 0.35$ with $\beta_2 = 2\beta_1$.

For detailed studies of the effect of the values of these control parameters on the stability and accuracy, we refer to Refs. [28,31]. The chosen values are only slightly different to those which give the standard Bathe method obtained when $\gamma = 0.5$ and $\beta_1 = 1/3$ with $\beta_2 = 2\beta_1$.

The parameters and values corresponding to $\gamma = 0.5$ and $\beta_1 = 0.35$, $\beta_2 = 2\beta_1$ in the β_1/β_2-Bathe scheme are in the ρ_∞-Bathe method $\gamma = 0.5$, $s_0 = s_1 = q_0 = q_1 = (1-\beta_1)/2 = 0.325$ and $s_2 = q_2 = \beta_1 = 0.35$ [29].

Our objective in the next sections is to present the numerical solutions of some challenging elastic wave propagation problems using the above solution schemes. The computed solutions provide insight into the important characteristics and limitations of the methods.

However, in addition, the problems may also serve as benchmark problems to evaluate the predictive capabilities of other numerical schemes for wave propagations.

5. Illustrative solutions: A one-dimensional wave propagation problem

We consider a clamped-free elastic bi-material bar, with zero initial conditions, subjected to a unit step load $H(t)$ at its free end, as described in Fig. 1. The bar has length $L = 4$ m and consists of two segments, each of the same length but with different materials for which the wave speeds are $c_1 = 40\sqrt{5}$ m/s and $c_2 = 20\sqrt{2}$ m/s, respectively. In what follows, we report on the time history of axial stress at the interface of the materials, point A; see Fig. 1.

This problem was studied using the linear finite elements with the standard and β_1/β_2 Bathe methods in Ref. [31] where it was demonstrated that the solutions reveal spurious oscillations and these oscillations can be suppressed to some extent by choosing good values of the parameters in the Bathe time integration methods. However, also, an accurate solution can be obtained in this case using the linear finite elements with the standard Bathe method when different uniform meshes are used in each material such that every element has the optimal CFL number (the CFL number is defined as CFL = cΔt/h, where c is the wave propagation velocity). We recall that for accurate solutions, the scheme using the linear finite elements and the standard Bathe method requires the optimal CFL number, CFL = 1. For this problem, we can easily achieve CFL = 1 throughout by setting $\Delta x_2/\Delta x_1 = c_2/c_1$ where Δx_1 and Δx_2 are the element lengths for the first and second materials, respectively and by choosing Δt = CFL $\Delta x_1/c_1$ with CFL = 1. Fig. 2 (a) shows the solution obtained using this approach with 190 elements and 600 elements for the first and second materials, respectively.

In general two- and three-dimensional problems, however, this optimality is impossible to achieve because waves propagating in different directions travel in essence through different element "lengths". The use of non-uniform meshes presents the same difficulty, as illustrated in Fig. 2(b) where a non-uniform mesh of N = 800 elements (400 elements for each material), each element with a different size (the size of each element is randomly chosen with $0 < \Delta x < 2L/N$), is used and an average wave speed and an average element length are employed to select the time step size Δt with CFL = 1. This difficulty limits the general use of the linear finite elements with the standard Bathe method.

The main attractive feature of the OFE-TRIn discretization is that the wave modes with $k_h h/\pi < n$ have practically no dispersion error regardless of the propagation direction [20]. Of course, the high-wavenumber wave modes with $k_h h/\pi > n$ need to be suppressed if they are excited, and one way is to exploit the numerical dissipation (the amplitude decay) property of implicit time integration methods. It should be, however, noted that the use of implicit time integration methods introduces additional dispersion errors caused by period elongation [20,26,27], and such waves need to be properly eliminated.

The use of the standard Bathe method with the OFE-TRIn discretization has shown to be desirable for some wave propagation problems [20]. However, for the problems in which many high-frequency waves are excited, like in the problems considered in this paper (propagations of discontinuous waves), the attenuation of high-frequency waves by the standard Bathe method is not sufficient to obtain an acceptable result. We present in Fig. 3(a) the solution of the bi-material bar problem calculated using the OFE-TRI3 and the standard Bathe method using a

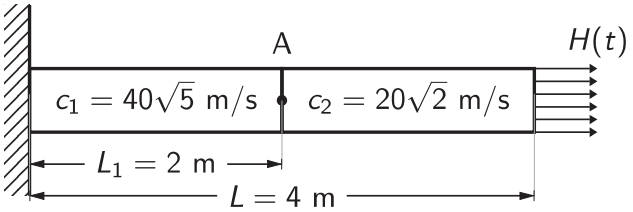

Fig. 1. An elastic bi-material bar impacted by a unit step axial pressure.

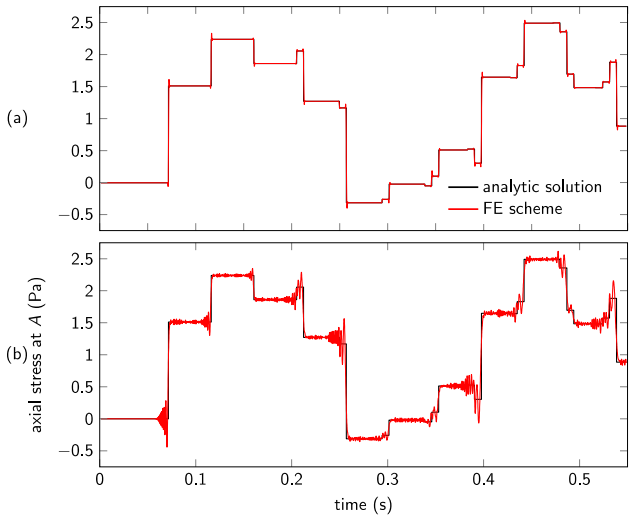

Fig. 2. Axial stress histories at the point A predicted by using the linear finite element with the standard Bathe method ($\gamma = 0.5$). (a) Uniform meshes of 190 elements and 600 elements (N = 790 in total) are used for the first and second materials, respectively, such that$\Delta x_2/\Delta x_1 \approx c_2/c_1$ and the time step size is set as Δt = CFL $\Delta x_1/c_1$ with CFL = 1. (b) A non-uniform mesh of N = 800 elements (400 elements in each material) is used and the time step size is set as Δt = CFL $2h/(c_1 + c_2)$ with h = L/N and CFL = 1. The non-uniform mesh is constructed by randomly distributing the nodes under the condition that the size of each element is $0 < \Delta x < 2L/N$.

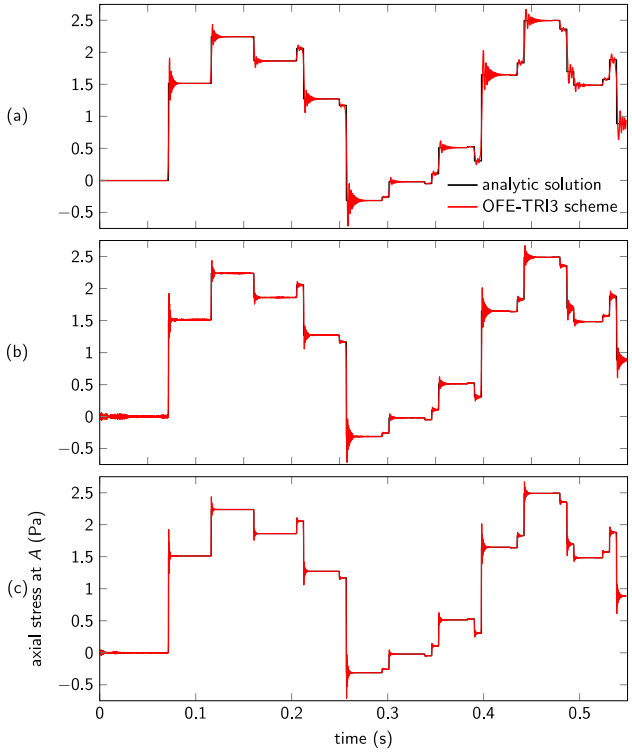

Fig. 3. Axial stress histories at the point A predicted by using the OFE-TRI3 with the standard Bathe method ($\gamma = 0.5$). A uniform mesh of N = 160 elements (80 elements in each material) is used and the time step size is set using (a) the wave speed of the second material (the smaller wave speed) and (b) that of the first material (the larger wave speed) both with CFL = 0.125. (c) A more refined uniform mesh of N = 640 elements (320 elements in each material) is used and the time step size is set using the larger wave speed with CFL = 0.125.

uniform mesh of 160 elements (80 elements in each material). We employed the wave speed of the second material to select the time step size with CFL = 0.125, and see that significant oscillations near the wave fronts occur. When the wave speed of the first material is adopted to choose the time step size, these oscillations slightly decrease, but additional oscillations arise ahead of the wave, as depicted in Fig. 3(b). These oscillations arise because while the wave modes with $k_h h/\pi < n$ are more accurately computed, those with $k_h h/\pi > n$ are not sufficiently suppressed. To alleviate these spurious oscillations, we may refine the mesh as shown in Fig. 3 (c) where 640 uniform elements are used (320 elements in each region), but the solution becomes computationally expensive.

The β_1/β_2-Bathe method enables to adjust the amount of numerical damping while introducing less error in the period elongation by choosing the parameters β_1, β_2 and γ. The best values of the parameters depend on the problem considered. We choose the values $\gamma = 0.5$ and $\beta_1 = 0.35$ with $\beta_2 = 2\beta_1$, because with these values the method exhibits sufficient numerical dissipation to suppress the spurious oscillations while keeping the dispersion error acceptably small. Fig. 4 shows the solutions of the bi-material bar problem using the OFE-TRI3 discretization with the β_1/β_2-Bathe method. Fig. 4(a) represents the solution when a uniform mesh of 160 elements (80 elements in each material) is used and the time step size Δt is set by the smaller wave speed with CFL = 0.125, where it is clearly seen that spurious oscillations are almost not present. An even more accurate solution can be obtained if the larger wave speed is used to select the time step size; see Fig. 4(b). It is also important to note that an accurate solution can be achieved even using non-uniform meshes, which may need to be employed in practical analysis; see Fig. 4(c). The predicted response in Fig. 4 shows excellent results obtained.

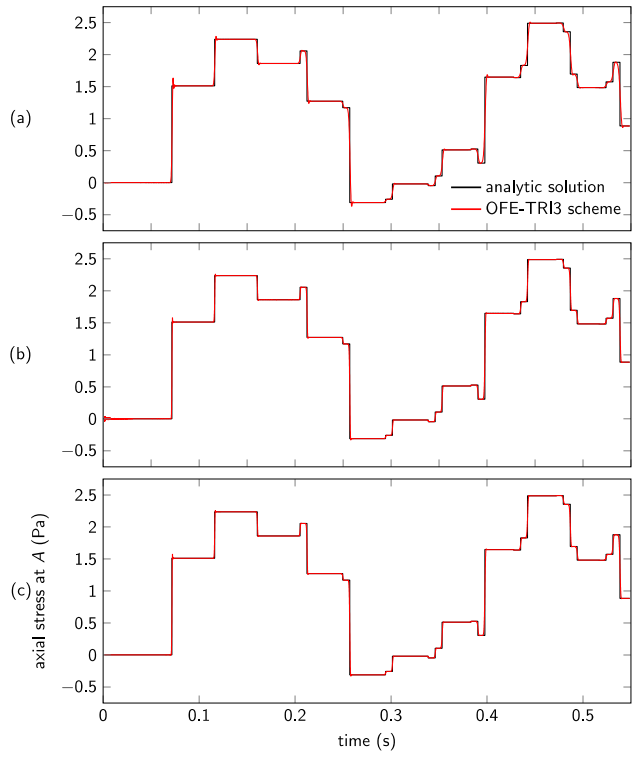

Fig. 4. Axial stress histories at the point A predicted by using the OFE-TRI3 with the β_1/β_2-Bathe method ($\gamma = 0.5$ and $\beta_1 = 0.35$ with $\beta_2 = 2\beta_1$), A uniform mesh of N = 160 elements (80 elements in each material) is used and the time step size is set using (a) the wave speed of the second material (the smaller wave speed) and (b) that of the first material (the larger wave speed) both with CFL = 0.125. (c) A non-uniform mesh of N = 160 elements (80 elements for each material) is used and the time step size is set as the larger wave speed with h = L/N and CFL = 0.125. The non-uniform mesh is constructed by randomly distributing the nodes with the condition that the size of each element is $0 < \Delta x < 2L/N$.

6. The solution of wave propagations through two-dimensional solids

In the previous section, several methods were used to solve a one-dimensional problem and it was discussed that the scheme using the OFE-TRI*n* and the β_1/β_2-Bathe time integration exhibited very attractive features: monotonic convergence with decreasing time step size and effective suppression of spurious high-frequency oscillations. In this section, the scheme is further applied to solve some computationally challenging problems, to obtain more insight but also to provide benchmark solutions for the evaluation of other computational procedures.

We solve the Lamb's problem [33], namely two-dimensional waves propagating in a semi-infinite elastic medium in plane strain conditions, as shown in Fig. 5. The isotropic elastic medium has mass density $\rho = 2200$ kg/m^3, Young's modulus $E = 1.8773 \times 10^{10}$ Pa, and Poisson's ratio $\nu = 0.25$, giving the P-wave velocity $c_P = 3200$ m/s, the S-wave velocity $c_S = 1847.5$ m/s, and the Rayleigh wave velocity $c_R = 1698.6$ m/s. The medium initially at rest is subjected to a line load concentrated at a point on the free surface, and the domain $V = [3200, 0] \times [0, 3200]$ is considered for the computation. We consider two types of loading, a Ricker wavelet and a set of step loadings, and always use the OFE-TRI2 element.

The time step size is based on the P-wave velocity with CFL = 0.125 and the element size is calculated as $h = \sqrt{2 \cdot 3200^2/N}$ where N is the number of elements. The displacements at two receivers located at $\boldsymbol{x} = (640, 0)$ and $\boldsymbol{x} = (1280, 0)$ are computed and compared to the analytical solutions given in Ref. [34].

6.1. The analysis of Lamb's problem subjected to a Ricker wavelet

We first consider a Ricker wavelet as the concentrated load, given by

$$F_c(t) = A\left[1 - 2\pi^2 \mathrm{f_p}^2 (\mathrm{t} - \mathrm{t_s})^2\right] e^{-\pi^2 \mathrm{f_p}^2 (\mathrm{t}-\mathrm{t_s})^2} \tag{32}$$

where we use $A = 2 \times 10^6$, $f_p = 10$ Hz, and $t_s = 0.1$ s.

We solve the problem using a uniform mesh of $N = 64 \times 64 \times 2 = 8,192$ elements (64 elements along each side of the computational domain), and a non-uniform mesh of $N = 5,000$ elements. The meshes are shown in Fig. 6. The results for the displacements at the two receivers are given in Fig. 7.

The modes of the elastic waves stimulated by the Ricker wavelet correspond to relatively low frequencies (compared to

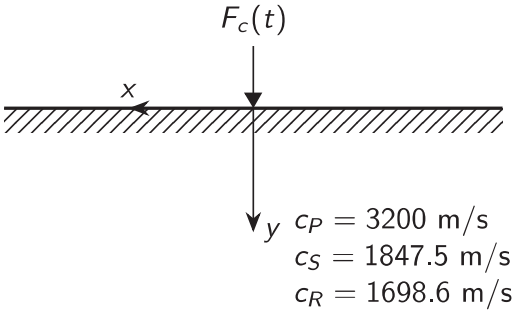

Fig. 5. A semi-infinite elastic medium in plane strain conditions subjected to a concentrated line force on the free surface.

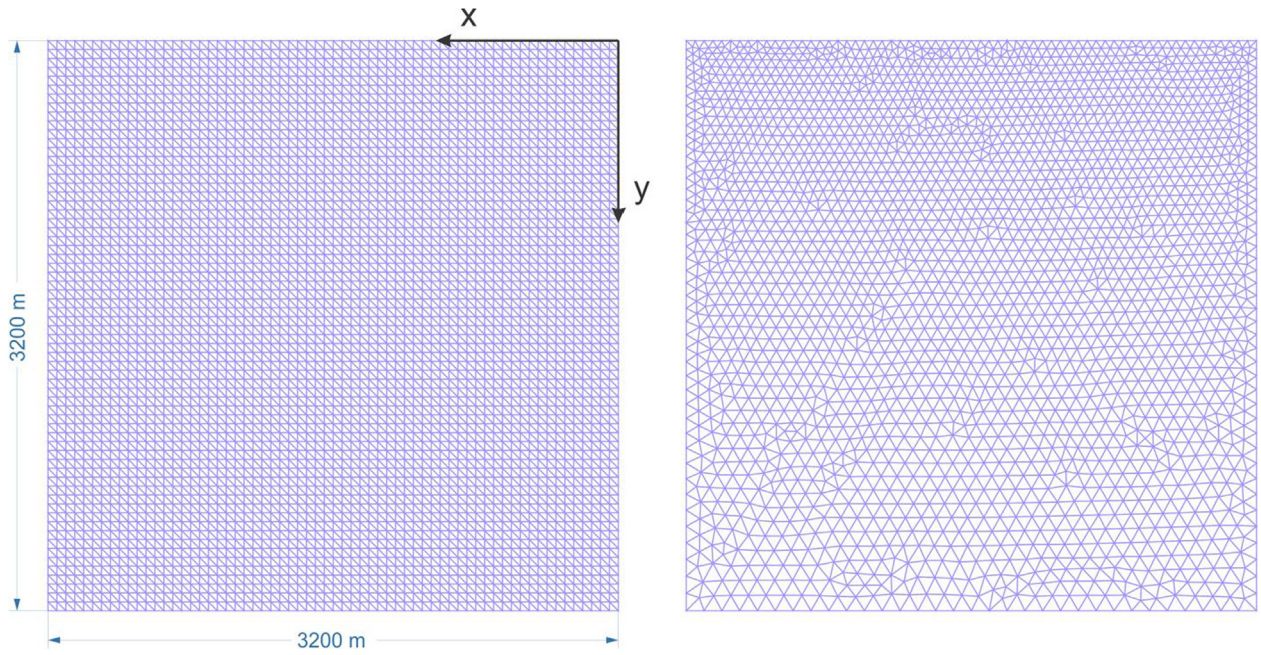

Fig. 6. A uniform mesh (left) and a non-uniform mesh (right) used for the Lamb's problem subjected to the Ricker wavelet. The numbers of elements are $N = 64 \times 64 \times 2 = 8,192$ and $N = 5,000$ in the uniform and the non-uniform meshes, respectively. In the non-uniform mesh, the element distribution is increasingly denser toward the free surface (two times denser than the distribution on the opposite boundary).

the wave modes from the step loadings considered in the following section). Hence, in this problem the standard Bathe method gives an accurate response prediction, and the numerical damping introduced by use of the β_1/β_2-Bathe method leads to a small amplitude decay in the solution, see Figs. 7 and 8.

6.2. The analysis of Lamb's problem subjected to step loadings

We next consider a concentrated line load consisting of three step functions, defined as

$$F_c(t) = 2 \times 10^6 [H(0.15 - t) - 3H(0.1 - t) + 3H(0.05 - t)] \tag{33}$$

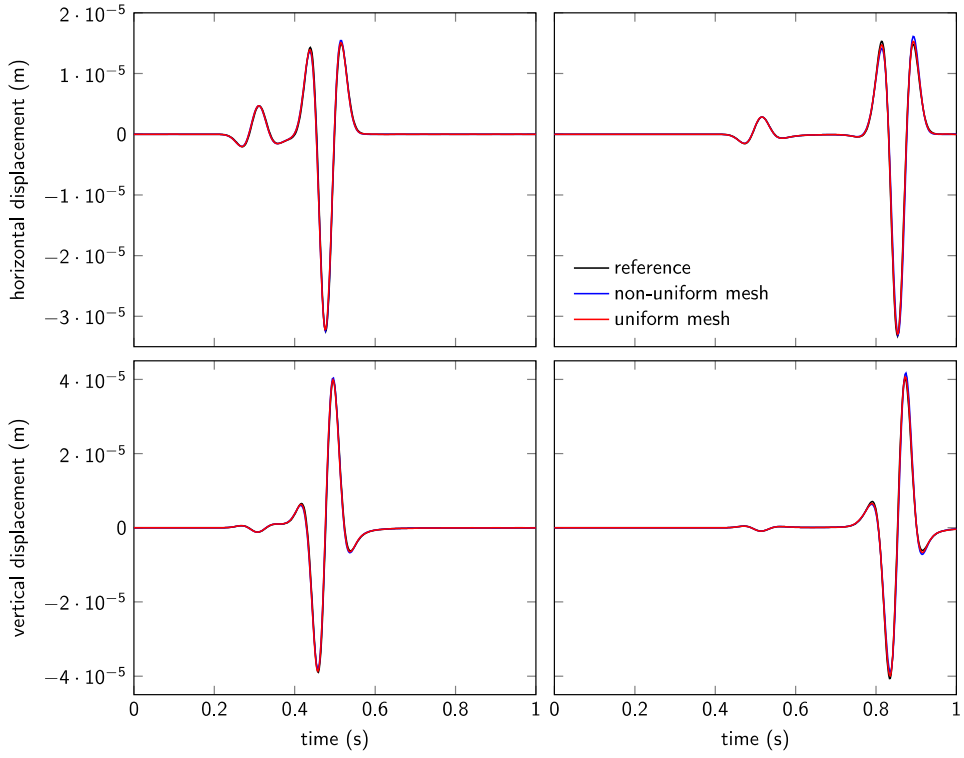

Fig. 7. Horizontal and vertical displacements of the elastic medium subjected to the Ricker wavelet on the free surface. The time histories of the displacements at $\boldsymbol{x}$ = (640,0) (left) and at $\boldsymbol{x}$ = (1280,0) (right) are shown. The OFE-TRI2 with uniform and non-uniform meshes (8,192 elements and 5,000 elements, respectively) and the standard Bathe method ($\gamma = 0.5$) with CFL = 0.125 are used. The analytical reference solution is based on Ref. [34].

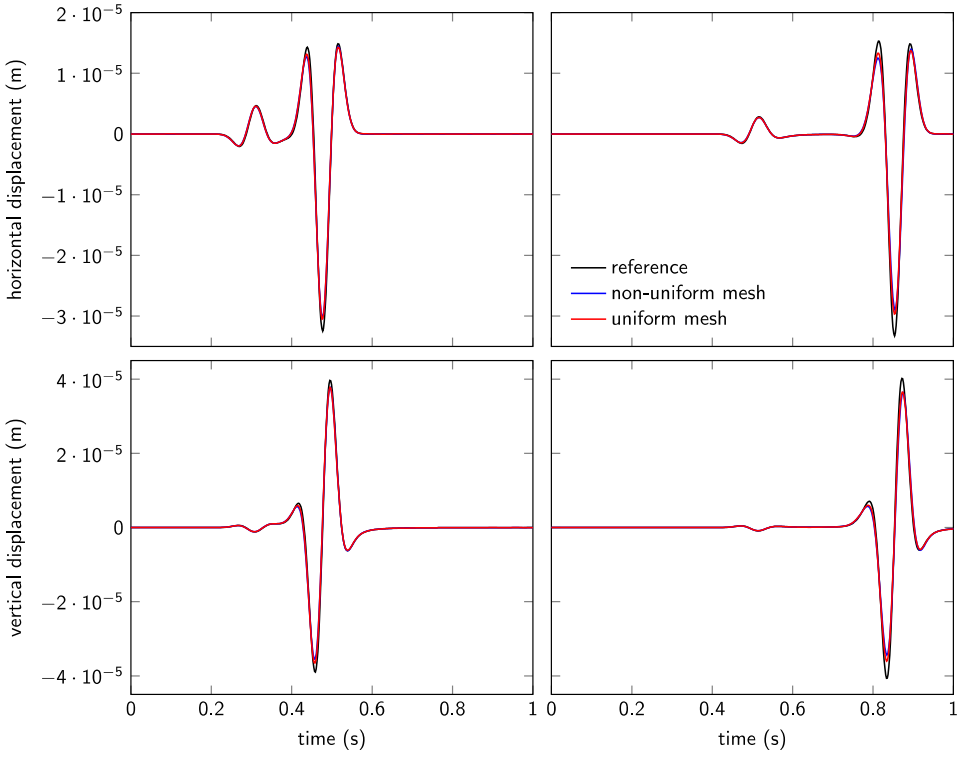

Fig. 6. A uniform mesh (left) and a non-uniform mesh (right) used for the Lamb's problem subjected to the Ricker wavelet. The numbers of elements are $N = 64 \times 64 \times 2 = 8,192$ and $N = 5,000$ in the uniform and the non-uniform meshes, respectively. In the non-uniform mesh, the element distribution is increasingly denser toward the free surface (two times denser than the distribution on the opposite boundary). We use symmetry of the problem with respect to the y-axis and solve for the response using the meshes described in the text and this figure. N always refers to the number of elements in the computational domain (like shown here).

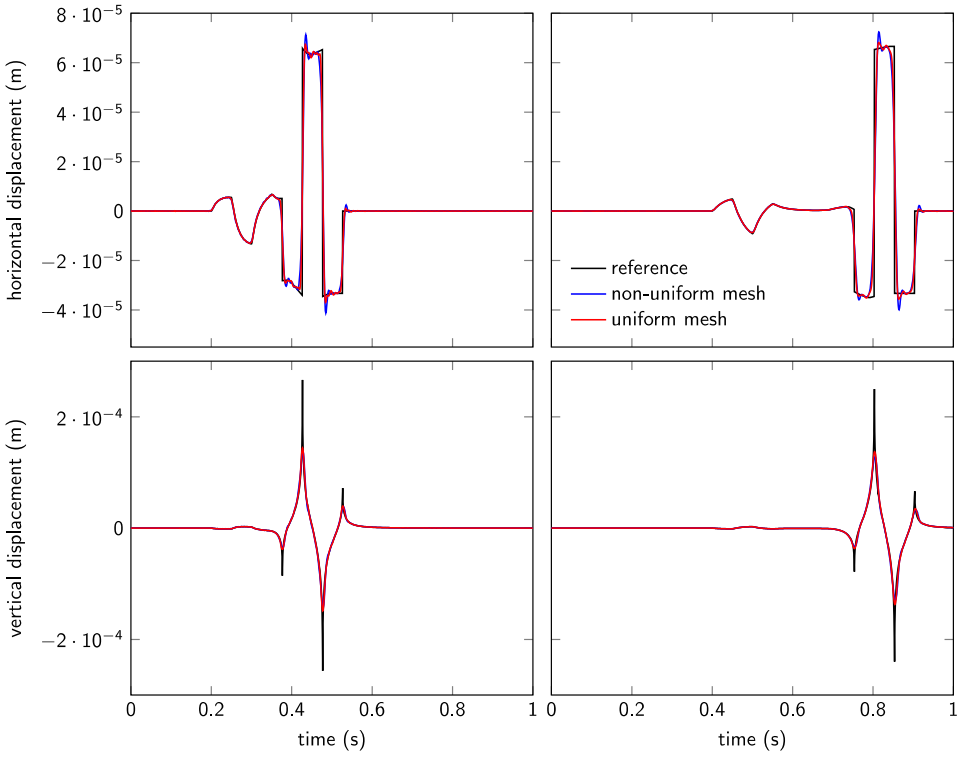

Fig. 9. Horizontal and vertical displacements of the elastic medium subjected to the step loading on the free surface. The time histories of the displacements at $\boldsymbol{x}$ = (640,0) (left) and at $\boldsymbol{x}$ = (1280,0) (right) are shown. The OFE-TRI2 with uniform and non-uniform meshes (51,200 elements and 30,446 elements, respectively) and the β_1/β_2-Bathe method ($\gamma = 0.5$ and $\beta_1 = 0.35$ with $\beta_2 = 2\beta_1$) with CFL = 0.125 are used. The analytical reference solution is based on Ref. [34].

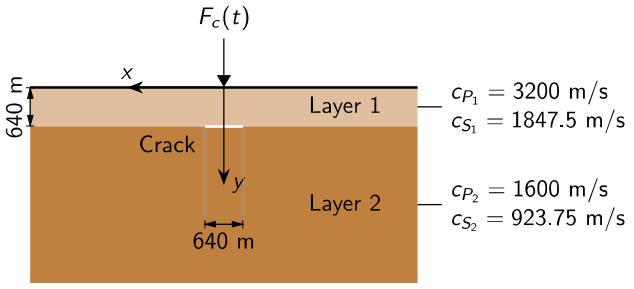

Fig. 10. A semi-infinite medium consisting of two elastic layers with a crack in plane strain conditions; a concentrated line force is applied on the free surface.

This discontinuous loading causes high-frequency wave modes, rendering the problem more difficult to solve. Hence we use finer meshes than in Section 6.1.

We use a uniform mesh of $N = 160 \times 160 \times 2 = 51,200$ elements and a non-uniform mesh of N = 30,446 elements where the nodes are increasingly denser toward the free surface; like in Fig. 6 for the coarse mesh used earlier. The calculated displacements at the two receivers are shown in Fig. 9, where it is seen that all the elastic waves are well predicted using the OFE-TRI2 with the β_1/β_2-Bathe method.

6.3. The solution of wave propagations through two media with a crack on the interface

Finally, we solve a wave propagation problem for which an analytical solution is not available. For this reason we use in each case three meshes (a coarse, finer and finest mesh).

The problem is described in Fig. 10: simulating multiple waves, triggered by a concentrated line force, traveling through a semi-infinite elastic medium in plane strain conditions, which consists of two elastic layers with a small crack between them. The first layer has the same material properties as before, i.e., the P-wave velocity $c_{P_1} = 3200$ m/s and the S-wave velocity

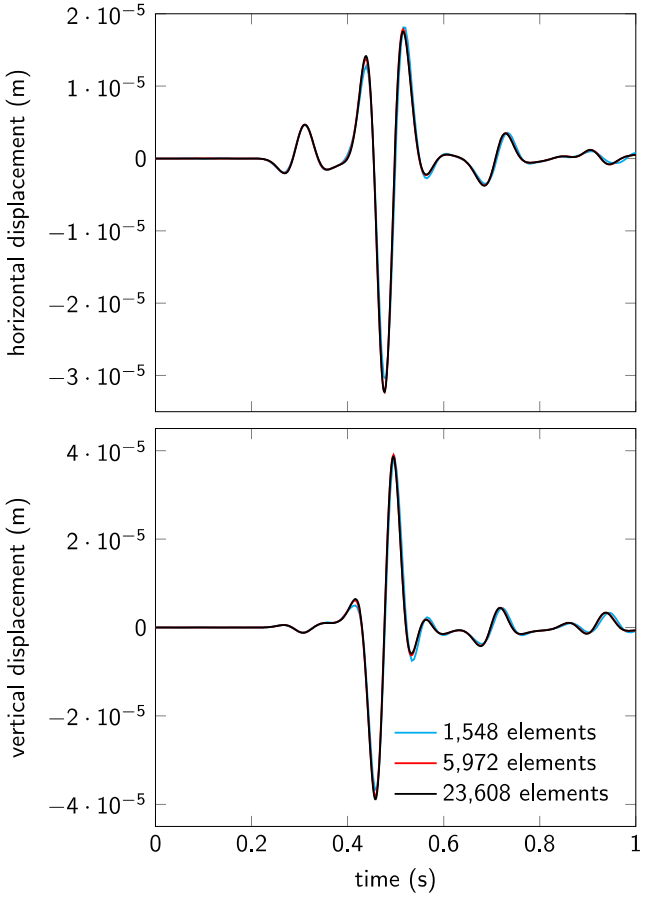

Fig. 12. Horizontal and vertical displacements of the two-layered elastic medium with a crack subjected to the Ricker wavelet on the free surface. The computed time histories of the displacements at $\boldsymbol{x} = (640, 0)$ are shown. The OFE-TRI2 with non-uniform meshes of 1,548 elements, 5,972 elements, and 23,608 elements and the standard Bathe method ($\gamma = 0.5$) with CFL = 0.125 are used.

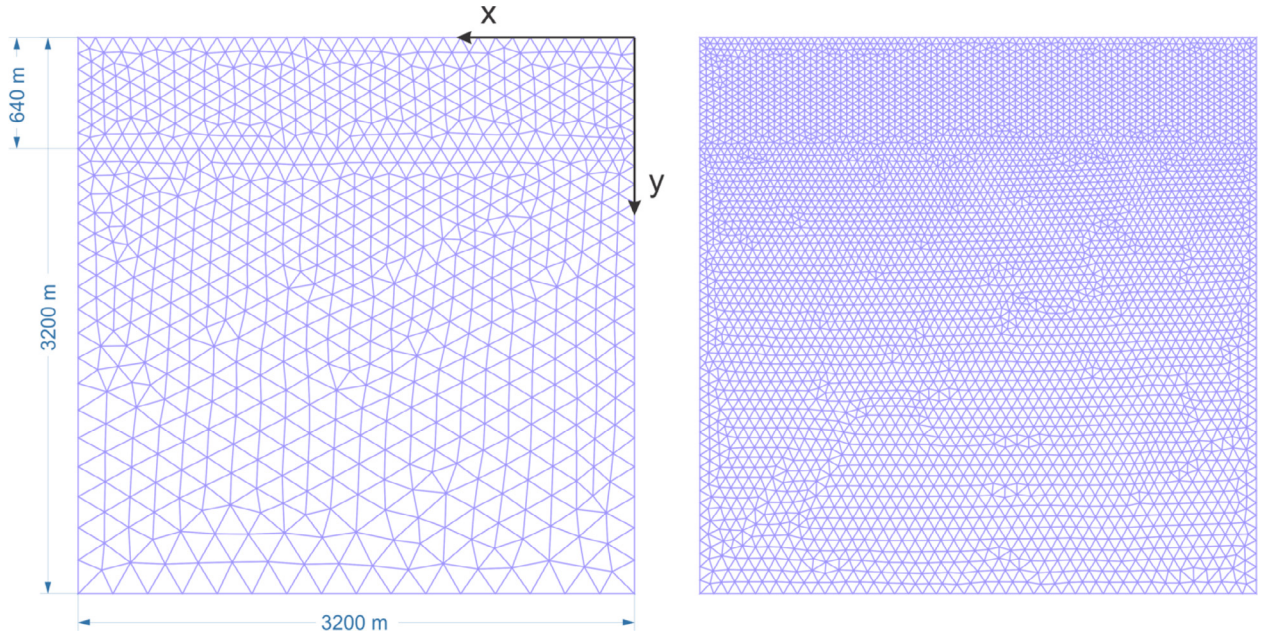

Fig. 11. The coarse meshes used for the two-media with a crack problem; the left is for the Ricker wavelet (1,548 elements) and the right is for the step loading (9,186 elements). The element distributions are increasingly denser toward the free surface (two times denser than on the opposite boundary).

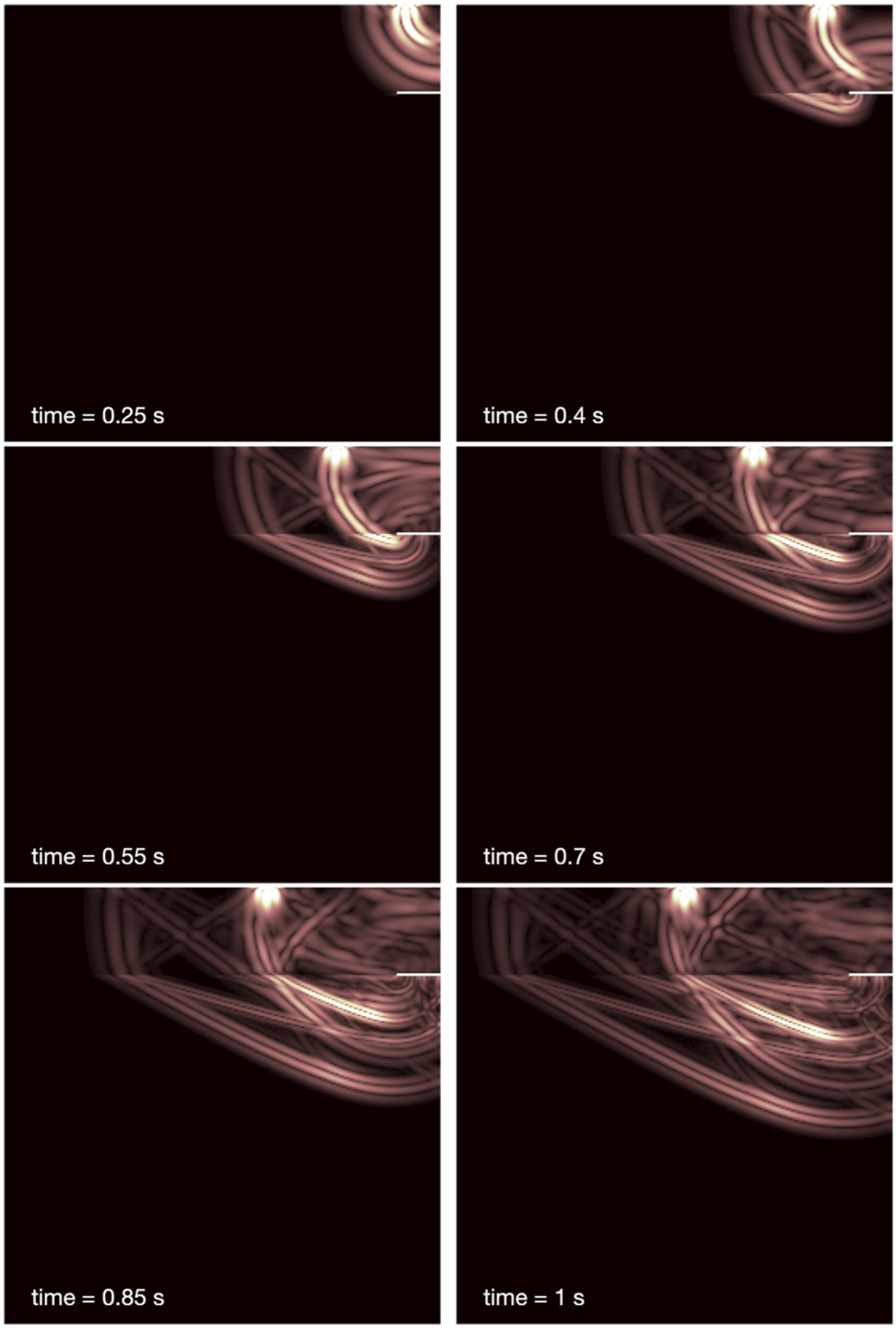

Fig. 13. Snapshots of von Mises stress distributions of the two-layered elastic medium with a crack at various observation times; the Ricker wavelet is applied on the free surface. The OFE-TRI2 with a non-uniform mesh of 5,972 elements and the standard Bathe method ($\gamma = 0.5$) with CFL = 0.125 are used.

$c_{S_1} = 1847.5$ m/s, but the second layer has a smaller Young's modulus $E_2 = 0.25E_1$, giving the P-wave velocity $c_{P_2} = 1600$ m/s and the S-wave velocity $c_{S_2} = 923.75$ m/s. The depth of the first layer and the length of the crack are both 640 m; see Fig. 10.

As before, we consider the Ricker wavelet and the step loading as the concentrated line force applied on the free surface. For the Ricker wavelet, we use the standard Bathe method since there are a limited number of wave modes excited; for the step loading,

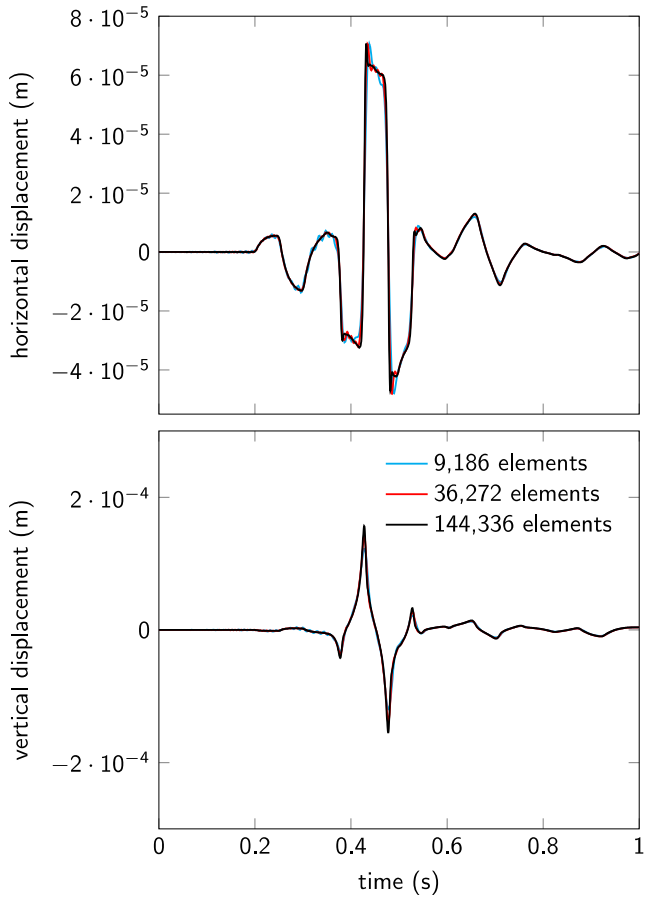

Fig. 14. Horizontal and vertical displacements of the two-layered elastic medium with a crack subjected to the step loading on the free surface. The time histories of the displacements at $\boldsymbol{x} = (640, 0)$ are shown. The OFE-TRI2 with non-uniform meshes of 9,186 elements, 36,272 elements, and 144,336 elements and the β_1/β_2 - Bathe method ($\gamma = 0.5$ and $\beta_1 = 0.35$ with $\beta_2 = 2\beta_1$) with CFL = 0.125 are used.

the β_1/β_2-Bathe method is employed to eliminate spurious high-frequency wave modes.

In this example, only non-uniform meshes are used. As in the previous examples, the meshes are gradually refined toward the free surface; see Fig. 11 for the coarse mesh case.

Fig. 12 shows the computed displacements at $\boldsymbol{x} = (640, 0)$ when the Ricker wavelet is applied, for which we use non-uniform meshes of 1,548, 5,972, and 13,378 elements. We observe that quite accurate solutions (measured on the finest mesh solutions) are obtained even with the coarse mesh. We also provide in Fig. 13 snapshots of the von Mises stress distributions at various observation times calculated using the mesh of 5,972 elements.

The free surface waves caused by the step loading are computed using non-uniform meshes of 9,186, 36,272, and 144,366 elements, and the results at $\boldsymbol{x} = (640, 0)$ are displayed in Fig. 14. While a more accurate solution is achieved as the mesh is refined, using the coarse mesh of 9,186 elements gives already reasonably accurate results (measured on the finest mesh solutions). Fig. 15 shows snapshots of the von Mises stress at selected time points.

7. Concluding remarks

In this paper, we elucidated and highlighted the features of using the overlapping finite elements and the Bathe time integration method in the analysis of elastic wave propagation problems. We focused on the effective use of the scheme to tackle some wave propagation problems that are difficult to solve accurately. Several challenging benchmark problems were solved to demonstrate the strengths of the procedures.

The crucial property of the scheme is that the solution accuracy increases monotonically as the time step size decreases and is independent of the propagation direction. Another important aspect is that the high-frequency wave modes that are not accurately calculated can be effectively removed by adjusting the parameters used in the Bathe time integration method. These features render the scheme suitable and desirable for the accurate simulation of wave propagations in general two- and three-dimensional solids with complex geometries.

The amount of the numerical dissipation to suppress the spurious oscillations in the solution should be appropriately adjusted depending on the problem considered. The overlapping finite elements with the standard Bathe method can perform well on problems where the solution is well approximated by low-frequency wave modes. However, if many high-frequency wave modes are excited, like by a discontinuous loading, it is very hard or perhaps even impossible to accurately represent the waves by just refining the spatial discretization and the time step size. In such cases, the spurious high-frequency waves need to be suppressed numerically without loss of solution accuracy in the waves that need to be well integrated, that is, the period elongation error should be small in these waves. The use of the β_1/β_2-Bathe method (or the ρ_∞-Bathe method) can be effective in this case.

In this paper, the parameter values for the β_1/β_2-Bathe method were chosen and kept at $\gamma = 0.5$ and $\beta_1 = 0.35$ with $\beta_2 = 2\beta_1$, for all problem solutions when the β_1/β_2-Bathe method was used. The values are only slightly different to those used in the standard Bathe method (for which $\gamma = 0.5$ and $\beta_1 = \frac{1}{3}$ with $\beta_2 = 2\beta_1$) and were chosen based on some numerical experiments and insight from the dispersion analysis given in Ref. [28]. While the values used here lead to accurate results in these problem solutions, we cannot say yet how good these values are for all solutions that may be considered.

Regarding the efficiency, we evaluated the computational cost involved in the scheme to some extent in Ref. [20]. However, a more exhaustive study solving various representative cases encountered in engineering practice would be of value.

Although we only considered one- and two-dimensional wave propagations, the analysis procedures used can be directly extended to three-dimensional solutions but the computational cost needs to be studied.

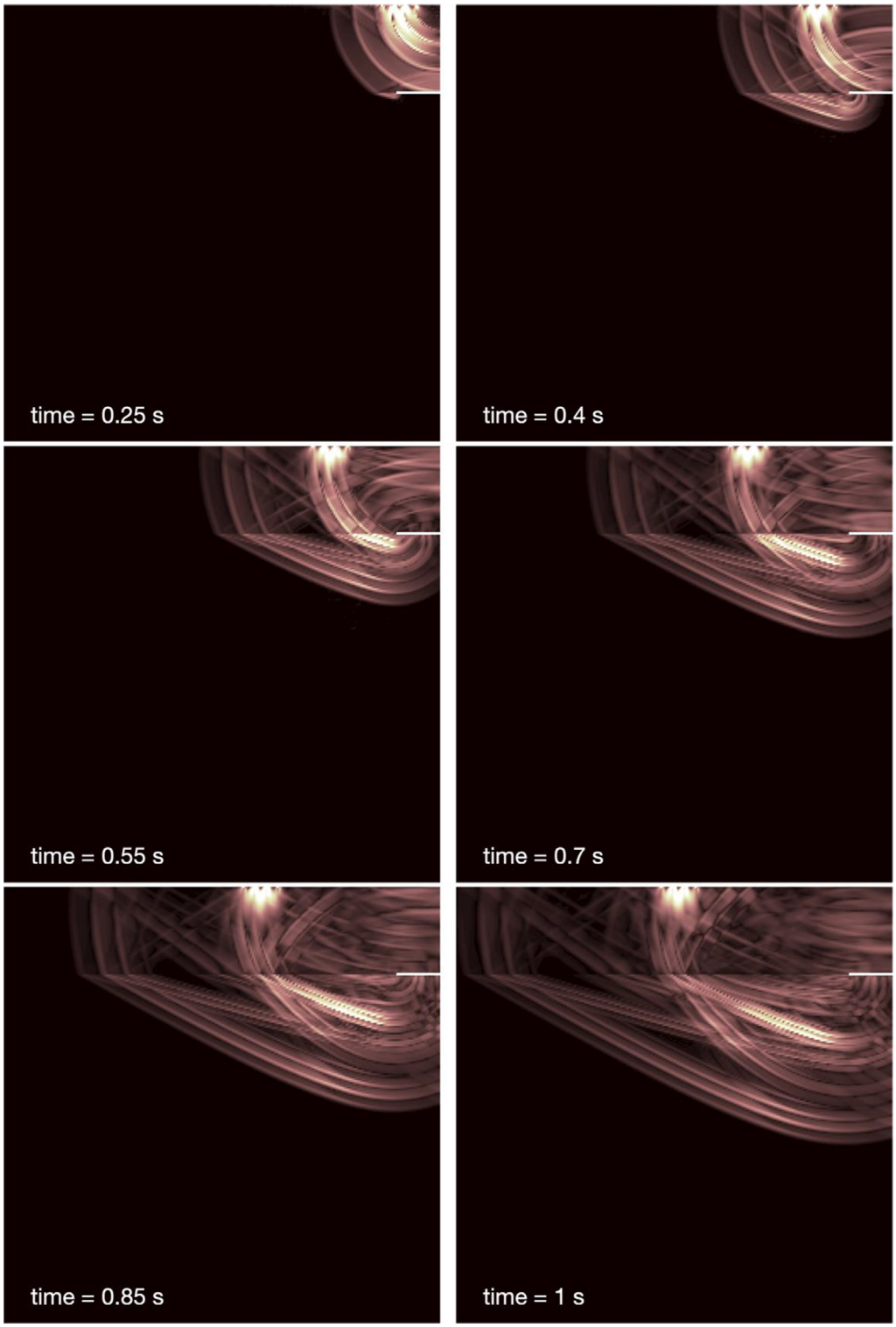

Fig. 15. Snapshots of von Mises stress distributions of the two-layered elastic medium with a crack at various observation times; the step loading is applied on the free surface. The OFE-TRI2 with a non-uniform mesh of 36,272 elements and the β_1/β_2 -Bathe method ($\gamma = 0.5$ and $\beta_1 = 0.35$ with $\beta_2 = 2\beta_1$) with CFL = 0.125 are used.

Declaration of Competing Interest

The authors declare that they have no known competing financial interests or personal relationships that could have appeared to influence the work reported in this paper.

References

[1] Graves RW. Simulating seismic wave propagation in 3D elastic media using staggered-grid finite differences. Bull Seismol Soc Am 1996;86 (4):1091–106.
[2] Aochi H, Ulrich T, Ducellier A, Dupros F, Michea D. Finite difference simulations of seismic wave propagation for understanding earthquake physics and

predicting ground motions: Advances and challenges. J Phys Conf Ser 2013;454:12010. https://doi.org/10.1088/1742-6596/454/1/012010.
[3] Sanes Negrete S, Muñoz-Cuartas JC, Vera-Ciro CA, van Dongen KWA. Modeling acoustic waves in locally enhanced meshes with a staggered-grid finite difference approach. Wave Motion 2020;98:102624. https://doi.org/10.1016/j.wavemoti.2020.102624.
[4] Bathe KJ. In: Bathe KJ, editor. Finite element procedures. Prentice Hall, 1996, 2nd ed. Watertown (MA); 2014 [also published by Higher Education Press China 2016].
[5] Ham S, Bathe KJ. A finite element method enriched for wave propagation problems. Comput Struct 2012;94–95:1–12. https://doi.org/10.1016/j.compstruc.2012.01.001.
[6] Komatitsch D, Tromp J. Introduction to the spectral element method for three-dimensional seismic wave propagation. Geophys J Int 1999;139(3):806–22. https://doi.org/10.1046/j.1365-246x.1999.00967.x.
[7] Witkowski W, Rucka M, Chróścielewski J, Wilde K. On some properties of 2D spectral finite elements in problems of wave propagation. Finite Elem Anal Des 2012;55:31–41. https://doi.org/10.1016/j.finel.2012.02.001.
[8] Galvez P, Ampuero J-P, Dalguer LA, Somala SN, Nissen-Meyer T. Dynamic earthquake rupture modelled with an unstructured 3-D spectral element method applied to the 2011 M9 Tohoku earthquake. Geophys J Int 2014;198(2):1222–40. https://doi.org/10.1093/gji/ggu203.
[9] Kim K-T, Bathe KJ. Transient implicit wave propagation dynamics with the method of finite spheres. Comput Struct 2016;173:50–60. https://doi.org/10.1016/j.compstruc.2016.05.016.
[10] Nicomedes WL, Bathe KJ, Moreira FJS, Mesquita RC. The method of finite spheres in acoustic wave propagation through nonhomogeneous media: Inf-sup stability conditions. Vietnam J Mech 2020;42(3):209–37.
[11] Nicomedes WL, Bathe KJ, Moreira FJS, Mesquita RC. Meshfree analysis of electromagnetic wave scattering from conducting targets: Formulation and computations. Comput Struct 2017;184:36–52. https://doi.org/10.1016/j.compstruc.2017.01.014.
[12] Ferroni A, Antonietti PF, Mazzieri I, Quarteroni A. Dispersion-dissipation analysis of 3-D continuous and discontinuous spectral element methods for the elastodynamics equation. Geophys J Int 2017;211(3):1554–74. https://doi.org/10.1093/gji/ggx384.
[13] He X, Yang D, Qiu C. Dispersion-dissipation analysis of triangular numerical-flux-based discontinuous Galerkin method for elastic wave equations. J Comput Phys 2020;418:109630. https://doi.org/10.1016/j.jcp.2020.109630.
[14] Yang Q, Shi Y, Ban ZG, Zhu SC. A nodal discontinuous galerkin time-domain method based on wave equation. IEEE Antennas Wirel Propag Lett 2020;19(7):1083–7. https://doi.org/10.1109/LAWP.2020.2988916.
[15] Guo N, Cawley P. Lamb wave reflection for the quick nondestructive evaluation of large composite laminates. Mater Eval 1994;52(3):404–11. https://www.osti.gov/biblio/7205126.
[16] Rose JL, Jiao D, Spanner JJ. Ultrasonic guided wave NDE for piping. Mater Eval 1996;54(11):1310–3. , https://www.osti.gov/biblio/418058.
[17] Bathe KJ. The finite element method with 'overlapping finite elements. Proceedings sixth international conference on structural engineering, mechanics and computation – SEMC 2016, 2016.
[18] Bathe KJ. The AMORE paradigm for finite element analysis. Adv Eng Softw 2019;130:1–13. https://doi.org/10.1016/j.advengsoft.2018.11.010.
[19] Zhang L, Kim K-T, Bathe KJ. The new paradigm of finite element solutions with overlapping elements in CAD – Computational efficiency of the procedure. Comput Struct 2018;199:1–17. https://doi.org/10.1016/j.compstruc.2018.01.003.
[20] Kim K-T, Zhang L, Bathe KJ. Transient implicit wave propagation dynamics with overlapping finite elements. Comput Struct 2018;199:18–33. https://doi.org/10.1016/j.compstruc.2018.01.007.
[21] Chai Y, Bathe KJ. Transient wave propagation in inhomogeneous media with enriched overlapping triangular elements. Comput Struct 2020;237:106273. https://doi.org/10.1016/j.compstruc.2020.106273.
[22] Huang J, Bathe KJ. Overlapping finite element meshes in AMORE. Adv Eng Softw 2020;144:102791. https://doi.org/10.1016/j.advengsoft.2020.102791.
[23] Huang J, Bathe KJ. On the convergence of overlapping elements and overlapping meshes. Comput Struct 2021;244:106429. https://doi.org/10.1016/j.compstruc.2020.106429.
[24] Bathe KJ, Baig MMI. On a composite implicit time integration procedure for nonlinear dynamics. Comput Struct 2005;83(31–32):2513–24. https://doi.org/10.1016/j.compstruc.2005.08.001.
[25] Bathe KJ. Conserving energy and momentum in nonlinear dynamics: A simple implicit time integration scheme. Comput Struct 2007;85(7–8):437–45. https://doi.org/10.1016/j.compstruc.2006.09.004.
[26] Bathe KJ, Noh G. Insight into an implicit time integration scheme for structural dynamics. Comput Struct 2012;98–99:1–6. https://doi.org/10.1016/j.compstruc.2012.01.009.
[27] Noh G, Ham S, Bathe KJ. Performance of an implicit time integration scheme in the analysis of wave propagations. Comput Struct 2013;123:93–105. https://doi.org/10.1016/j.compstruc.2013.02.006.
[28] Malakiyeh MM, Shojaee S, Bathe KJ. The Bathe time integration method revisited for prescribing desired numerical dissipation. Comput Struct 2019;212:289–98. https://doi.org/10.1016/j.compstruc.2018.10.008.
[29] Noh G, Bathe KJ. The Bathe time integration method with controllable spectral radius: The ρ_∞-Bathe method. Comput Struct 2019;212:299–310. https://doi.org/10.1016/j.compstruc.2018.11.001.
[30] Kwon S-B, Bathe KJ, Noh G. An analysis of implicit time integration schemes for wave propagations. Comput Struct 2020;230:106188. https://doi.org/10.1016/j.compstruc.2019.106188.
[31] Malakiyeh MM, Shojaee S, Hamzehei-Javaran S, Bathe KJ. New insights into the β_1/β_2-Bathe time integration scheme when L-stable. Comput Struct 2021;245:106433. https://doi.org/10.1016/j.compstruc.2020.106433.
[32] Noh G, Bathe KJ. An explicit time integration scheme for the analysis of wave propagations. Comput Struct 2013;129:178–93. https://doi.org/10.1016/J.COMPSTRUC.2013.06.007.
[33] Lamb H. On the propagation of tremors over the surface of an elastic solid. Philos Trans R Soc Lond Ser A, Contain Pap Math Phys Charact 1904;203:1–42. http://www.jstor.org/stable/90855.
[34] Miklowitz J. The theory of elastic waves and waveguides. New York (NY): North Holland; 1978.